Devitrification of colloidal glasses in real space

Nikoleta B. Simeonova, Roel P. A. Dullens, Dirk G. A. L. Aarts, Volkert W. A. de Villeneuve, Henk N. W. Lekkerkerker, and Willem K. Kegel*

Van 't Hoff Laboratory for Physical and Colloid Chemistry, Debye Institute, Utrecht University, Padualaan 8, 3584 CH Utrecht, The Netherlands

(Received 11 October 2005; revised manuscript received 2 December 2005; published 5 April 2006)

Confocal scanning laser microscopy has been used to quantitatively analyze the structure and dynamics of concentrated suspensions of spherical colloids in which the magnitude of the short-range attractive potential is increased by adding nonadsorbing polymers. These systems undergo a reentrant glass transition upon increasing polymer concentration. We find that melting of the glass is accompanied by significant changes in the displacement distribution and its moments. However, no significant variations have been detected in the shapes of the displacement distributions. Moreover, structural correlation functions and the magnitude of local density fluctuations do not vary significantly between the glass states and the fluid. Considering our experimental setup, these observations imply that local density fluctuations cannot be larger than a few percent of the average density.

DOI: 10.1103/PhysRevE.73.041401 PACS number(s): 82.70.Dd, 64.70.−p, 05.40.Jc

I. INTRODUCTION

Understanding the structure and stability of glasses and gels is among the major challenges in statistical physics. Glasses and gels are solids without long-range positional order. A wide variety of molecular and macromolecular systems form glasses; see, e.g., Ref. [1] for an overview. A glass state has also been observed in colloidal systems in which only excluded volume interactions play a role; see, e.g., Refs. [2,3]. Colloidal gels often form at relatively low volume fractions of colloids, but only if short-range attraction is present, see, e.g., Ref. [4]. It has recently become clear, by theory [5], experiments [6–8], and computer simulation [9], that glasses of colloidal hard spheres can be "devitrified" upon increasing attraction between the colloidal particles. By devitrification we mean that structurally disordered systems that do not reach long-time self-diffusion within experimental time scales do so after "switching on" the attraction. Attraction between colloidal particles can be accomplished by adding nonadsorbing polymers, leading to an attractive potential (of mean force) between the colloids [10,11]. Interestingly, the system again forms a glass state if even more polymer is added [6,7]. The situation is shown schematically in Fig. 1. In Refs. [7,8] it has been shown that the peak of the static structure factor shifts to slightly larger q values when the repulsive glass devitrifies. At the same time, the extrapolated value of the static structure factor at $q=0$ increases. These observations point to local inhomogeneities of the particle density: the shift of the peak of $S(q)$ suggests a decreasing interparticle distance, while the larger values of $S(q=0)$ suggest an increasing osmotic compressibility. At constant volume, decreasing interparticle distance indeed should locally induce holes of relatively low number densities. Dynamically, this translates into a subset of particles becoming more mobile at the expense of another subset. In this work, this scenario is investigated by analyzing the particle displacement distributions as well as the local particle density distibutions using Voronoi constructions.

II. EXPERIMENTAL SECTION

We used polymethyl methacrylate spheres consisting of a fluorescent core and a non-fluorescent shell and a relative polydispersity of 6% [12,13]. The particles were dispersed in a refractive-index-matching solvent mixture of *cis*-decalin ($C_{10}H_{18}$, Merck, for synthesis), tetralin ($C_{10}H_{12}$, Merck, for synthesis), and carbon tetrachloride (CCl_4, Merck, for spectroscopy) with volume fractions of 0.315, 0.36, and 0.325, respectively. The mass density of this solvent mixture is close to that of the particles with a mismatch of $\Delta\rho=0.02$ g/cm^3 and the interparticle interactions are hard [14,15]. The diameter d of the particles is 1.45 μm, corresponding to a gravitational length $h=6kT/(\Delta\rho d^3 g)\approx 13$ μm with g the acceleration due to gravity. The volume fraction ϕ of the colloids was 0.59 as determined relative to the random close-packed volume fraction as in Ref. [14]. Samples contained several concentrations of nonadsorbing polymer poly-

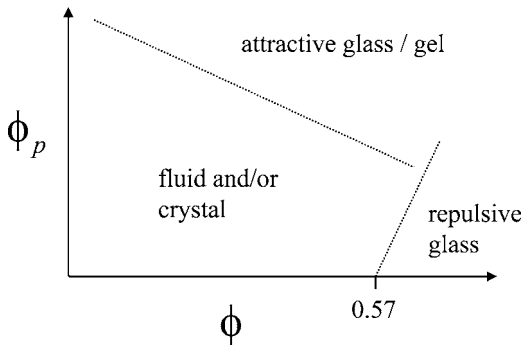

FIG. 1. Schematic stability diagram of fluid, repulsive glass and attractive glass or gel state as a function of colloid volume fraction ϕ and polymer volume fraction ϕ_p. Modeled after Ref. [6–8]. At constant $\phi \geqslant 0.57$ and increasing ϕ_p, a sequence repulsive glass-fluid-attractive glass is observed, referred to as a reentrant glass transition.

*Electronic address: W.K.Kegel@chem.uu.nl

styrene (Fluka; molecular weight 6×10^5 g/mole; radius of gyration $r_g\approx22$ nm). The volume fractions of the polymer ϕ_p ($=4\pi r_g^3\rho/3$ with ρ the polymer number density) are equal to 0, 0.010, 0.036, 0.042, 0.063, 0.10, and 0.23. Without polymer, the typical time scale in the system is the Brownian time defined by $\tau_B=R^2/6D_0=1.61$ s. Here, R is the radius of a colloidal particle and D_0 is its diffusion coefficient at infinite dilution and no polymer. The last quantity is given by $D_0=kT/6\pi\eta_0R$, with η_0 the solvent viscosity. Increasing polymer is expected to increase the viscosity η of the samples, as a first approximation via the Einstein relation $\eta=\eta_0(1+2.5\phi_p)$. This implies that the difference in viscosity between the samples with $\phi_p=0.23$ and $\phi_p=0$ is roughly 50%. Samples were prepared by mixing stock solutions of colloid and polymer. After mixing, the samples have been continuously tumbled for at least three days. Measurements started within one hour after tumbling was finished.

A Nikon TE 2000U inverted microscope equipped with a Nikon C1 confocal scanning head in combination with a HeNe laser (5 mW, 543 nm, Melles Griot) and an oil-immersion lens (100× CFI Plan Apochromat, NA 1.4, Nikon) was used to image the particles. The two-dimensional (2D) *xy*-cross-section images of approximately 30 particle diameters away from the wall of the sample cell had a resolution of 512×512 pixels and the frame size was 50×50 μm^2. The optical thickness of a slice, before image analysis, was 0.5 particle diameters. The scan speed was about 1 s per frame. The centers of the particles were located using particle tracking routines based on those described in [16]. With this procedure, under optimal conditions a resolution of particle positions of approximately 1/10 of a pixel can be accomplished. Time series were taken over 150 intervals of 30 s.

A. Dynamics

From the retrieved particle positions we determined several properties. First of all, we calculated the self-part of the van Hove correlation function G_s, being the canonically averaged probability distribution that a particle has traveled a distance x in a time interval t:

$$G_s(x,t)=\frac{1}{N}\left\langle\sum_{i=1}^{N}\delta[x+x_i(0)-x_i(t)]\right\rangle. \tag{1}$$

Subsequently, the mobility of the particles was measured in terms of the mean squared displacement $\langle x^2\rangle$, which is defined as the second moment of G_s:

$$\langle x^2(t)\rangle=\sum_{i=1}^{N}x^2(t)G_s(x,t). \tag{2}$$

Here and below, all distances are given in units of the particle diameter, unless stated otherwise.

The lowest-order deviation from a Gaussian displacement distribution for displacements along a single coordinate is given by [17]

$$\alpha_2(t)=\frac{\langle x^4(t)\rangle}{3\langle x^2(t)\rangle^2}-1. \tag{3}$$

B. Structure

From the particle positions we calculated the radial distribution function and the Voronoi "volumes." The radial distribution function $g(r)$ (being proportional to the probability of observing a particle at distance r away from a given particle) is given by

$$g(r)=\frac{1}{\rho^2}\left\langle\sum_i\sum_{j\neq i}\delta(\vec{r}_i)\delta(\vec{r}_j-\vec{r})\right\rangle, \tag{4}$$

with ρ the average number density. The indices i and j run over all particles. The nearest neighbors of every particle were identified by correlating the particle positions within single frames using a Delaunay triangulation. Using the corresponding Voronoi polygon construction (a Voronoi cell for each particle is defined as the region of space closer to that particle than it is to any other particle), the local area (note that we are dealing with 2D slices) occupied by a single particle, A_v, was determined. We define the normalized local area as

$$a_v=\frac{A_v}{\pi R^2}, \tag{5}$$

and compute the distribution of a_v, $p(a_v)$; the results are presented in Sec. III.

III. RESULTS AND DISCUSSION

In Fig. 2 the displacement distributions Eq. (1) at three different times and for three different polymer concentrations are shown. The distributions clearly are dynamically heterogeneous, being manifested in non-Gaussian displacement distributions as has also been observed in [14,18] for concentrated suspensions of hard colloidal spheres.

As is obvious from Fig. 2, increasing the volume fraction of polymer from $\phi_p=0.013$ to 0.063 devitrifies the colloidal hard-sphere glass. Increasing the polymer concentration even further, i.e., to 0.23, the system again becomes more or less immobile. As can be seen in the figure, at $t=150$ s the displacement distributions of all three polymer concentrations are still indistinguishable. At longer times, however, at least beyond 300 s, the displacement distribution of the system with $\phi_p=0.063$ is substantially broader than samples with both higher and lower polymer concentrations. Thus, the mobility in the sample with intermediate polymer is significantly higher than in the other samples. This can be verified in Fig. 3, where we plotted the mean squared displacements Eq. (2) as a function of time. Both figures show that an additional increase of the polymer concentration slows down the system again. We note that the uncertainty in the data in Fig. 3 is large, caused by the mean-squared displacement being a second moment of the displacement distribution. By these observations we verify the reentrant glass transition as a function of polymer concentration, as also observed experimentally in Ref. [6,7]. At small polymer concentration, the system is a repulsive glass. Upon increasing polymer concentration the system devitrifies, followed by a second (reentrant) glass transition upon further increase of the polymer concentration.

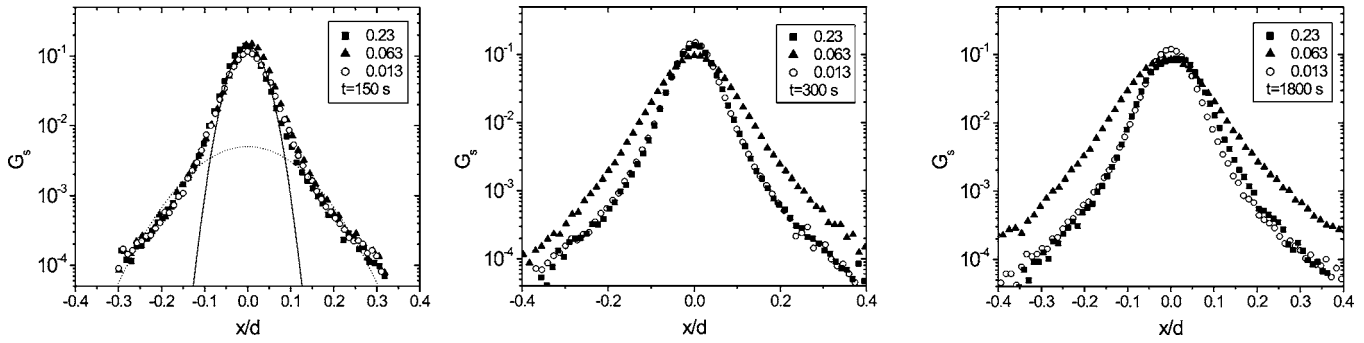

FIG. 2. Displacement distributions Eq. (1), at three different times, for samples with colloid volume fraction of 0.59, and three different polymer concentrations 0.013, 0.063, and 0.23 as indicated in the figure. Solid lines are Gaussian fits to the (arbitrary) slow and fast subsets of the particles.

We now address the question of whether devitrification is accompanied by increased deviations from Gaussian displacement distributions compared to the dynamically arrested systems. Such deviation is quantified by the value of the non-Gaussian parameter α_2 in Eq. (3). If devitrification was caused by a subset of particles becoming more mobile at the expense of another subset, a scenario that has been discussed in the Introduction, then a significantly larger value of α_2 would be expected in the system with $\phi_p=0.063$. This obviously is not the case; as can be seen in Fig. 4, in all systems, the value of α_2 as a function of mean-squared displacement fall on the same curve with a (shallow) maximum around $\langle x^2\rangle \approx 0.01$. This behavior is corroborated by inspection of the particle trajectories (not shown).

In Fig. 5 we show typical configurations of the repulsive glass, the devitrified sample and the attractive glass. From qualitative inspection of these snapshots, one would not be able to tell which sample corresponds to what dynamic situation in Figs. 2 and 3. In the devitrified samples, crystalline regions were observed several weeks after preparation, but no systematic crystallization study (as in Refs. [6,8]) has been carried out. We will now analyze the structure and the local volume distributions of the systems.

The pair correlation functions $g(r)$ [see Eq. (4)] are shown in Fig. 6 and the Voronoi distributions are given in Fig. 7. Clearly, these quantities do not point to significant differences in the real-space structure in these systems. At least in more dilute systems, the first peak of $g(r)$ is expected to sharpen with increasing polymer concentration [19], which is not observed in the dense systems studied here. Neglecting excluded volume effects of the polymers, the depth of the attraction wells as a function of polymer concentration is given by $-\beta u = 1/2\ \phi_p(3/\xi+2)$ with $\xi=2r_g/d$; see, e.g., [20]. It is easy to verify that $\phi_p \approx 0.013$, 0.036, 0.042, 0.063, 0.1, and 0.23 correspond to $-\beta u \approx 0.7$, 1.8, 2.1, 3.2, 5.0, and 11.5, respectively. Comparing these numbers with the results in Figs. 2 and 3 reveals that devitrification occurs when the depth of the attraction well $-\beta u \approx 2-3$, while the attractive glass forms when $-\beta u \approx 3-5$. From the data in Ref. [8] we deduce, at a colloid volume fraction of 0.6, $-\beta u \approx 0.7$ and $-\beta u \approx 1.6$ for the devitrification and reentrant glass transition, respectively. These numbers are significantly smaller compared to those extracted from our data. This may be caused by different ranges of attraction induced by the polymers of different radius of gyration in the two experimental setups. Indeed, in Ref. [8], $\xi=0.09$ while in our experiments, $\xi=0.03$. This points to the fact that the sequence repulsive glass–devitrified state–reentrant glass is shifted to lower polymer concentrations upon increasing the range of interac-

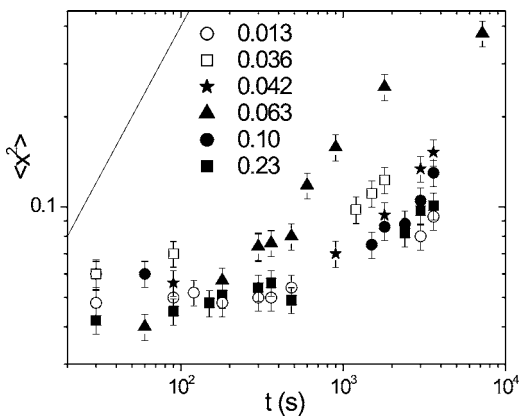

FIG. 3. Mean-squared displacements calculated by Eq. (2) for systems with constant volume fraction of colloid (0.59) and increasing polymer concentration. The solid line has unit slope and represents the long-time diffusion limit.

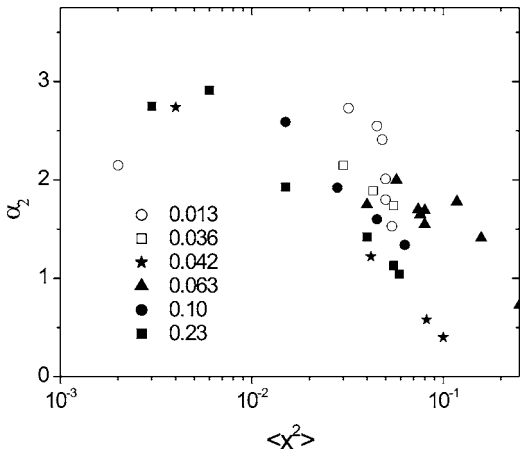

FIG. 4. Values of the non-Gaussian parameter α_2, given by Eq. (3), as a function of the mean-squared displacement; symbols as in Fig. 3.

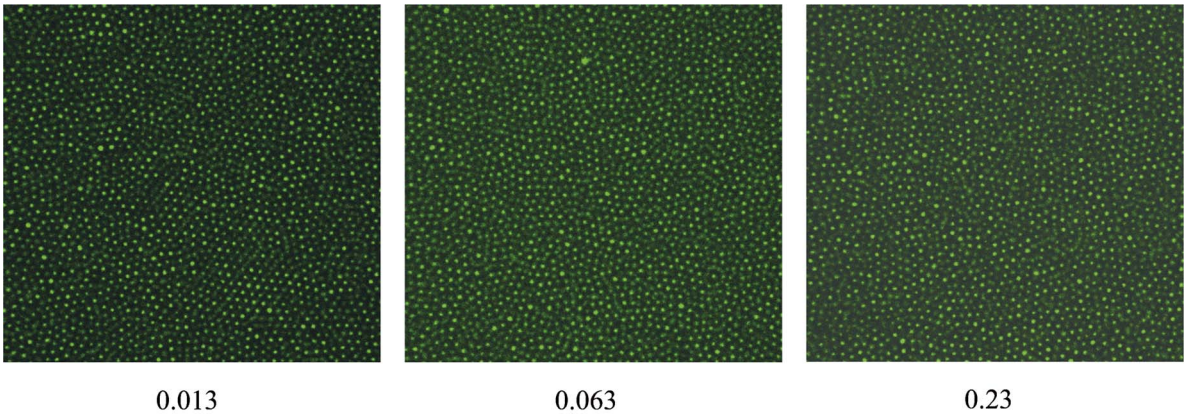

FIG. 5. (Color online) Snapshots of systems with different volume fractions of polymer, as indicated. From left to right we have a repulsive glas, devitrified state, and reentrant glass.

tions. This scenario seems globally in agreement with theory; see Ref. [5].

As mentioned in the Introduction, in Ref. [8] it has been observed that increasing the polymer concentration in the system is accompanied by a shift in the structure factor peak to higher q as well as an increased osmotic compressibility. Upon increasing polymer concentration, these observations may translate into local clustering of particles which, at constant volume, opens up "holes" on the spatial scale of a few particle diameters. In real space, this scenario should be reflected in (1) smaller spacing in the peaks of $g(r)$; (2) broadening in the distribution of Voronoi volumes, or a bimodal distribution of Voronoi volumes. In the last situation, local clustering leads to smaller Voronoi volumes, and the holes lead to larger volumes. It can be verified that the shift of the structure factor peak as observed in Ref. [8] corresponds to roughly 5% of the particle diameter. Such a small difference will indeed not show up in our measured $g(r)$. Whether it shows up in the distribution of Voronoi volumes depends on the spatial scale of the inhomogeneities. This scale is hidden in the osmotic compressibility, but cannot be extracted from the data in Ref. [8]. The results in Fig. 7 show that inhomogeneities in interparticle spacing—if any—are below the experimental resolution of the Voronoi volumes. We measured the standard deviation of the positions of the particles under slightly different values of the parameters used in our tracking procedure. These values were chosen in such a way that visually, all particle positions were recovered. With this procedure, we verified that the resolution of the particle positions in our datasets is 1/4 to 1/3 of the size of a pixel (with a size of 50/512 μm), or 25–35 nm, 2% of the particle diameter. Voronoi volumes are based on interparticle distances which are in fact projected distances in a vertical slice of finite thickness. The uncertainty in the interparticle distance extracted from these slices may be significantly larger. The thickness of an optical slice is "normalized" by using refractive-index-matched solvent, the same microscopy settings in all experiments, and averaging over several experimental samples. We moreover reduced the optical thicknesses by disciminating all particles with intensity below 50% of the average intensity. With these precautions, the effect of finite slice thickness contributes as a systematic error showing up, e.g., in finite contributions to $g(r<d)$ in Fig. 6 and in finite $p(a_v<1)$. Distributions of (averaged) interparticle distances are therefore expected to significantly detect shifts larger than roughly 30 nm.

We have also analyzed our data in terms of "bond" distance distributions. In fact, the $g(r)$'s in Fig. 6 are radial

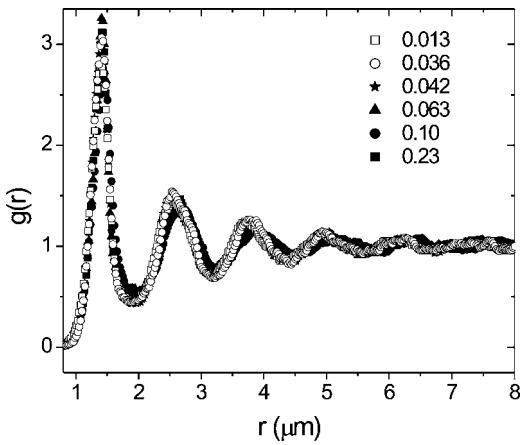

FIG. 6. Radial distribution functions of the same systems as in previous figures.

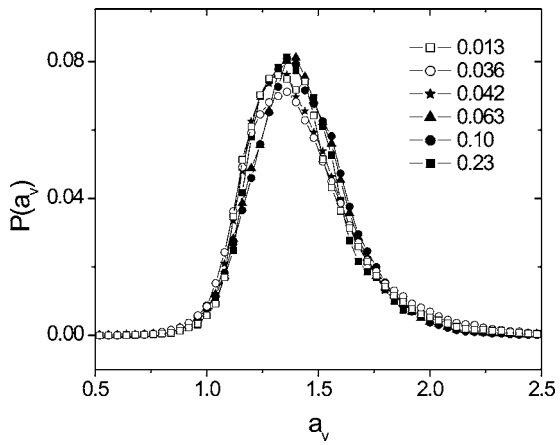

FIG. 7. Distribution of Voronoi volumes in the same systems as in previous figures.

averages over these distributions. A radial average is not very sensitive for "clustering" in the form of pairs or linear aggregates of the colloids. However, by comparing the distributions of interparticle distances (not shown), no significant differences showed up. This implies that shifts in local bond distibutions are below the experimental resolution of the particle positions, again estimated as 30 nm. How does that compare to the shift of the structure factor corresponding to about 5% of the particle size as observed in Refs. [7,8]? For the particle size we used here, this difference, in our case about 60–70 nm, should show up in the Voronoi distribution Fig. 7 as well as in the distribution of interparticle distance. The interparticle distance scales as $l=d(\phi_{rcp}/\phi)^{1/3}$ with ϕ_{rcp} the random close packed volume fraction of 0.64. From that, it is easy to see that differences in volume fraction on the order of 0.01 give rise to differences in interparticle distance of order 1%. Thus, a small uncertainty in volume fraction may partly account for the significant shift of the structure factor peak in Refs. [7,8]. On the other hand, two independent experiments [7,8] show the same trend, thereby adding weight to the significance of the shift of the structure factor. The systematic increase of osmotic compressibility with polymer concentration as observed in Refs. [7,8] points to increased density fluctuations in the system. These fluctuations have not been detected by our experimental setup, implying that the relative fluctuations in density are smaller than 2–3% of the interparticle distances. In ending this section, we note that in Ref. [21] a significant influence of gravity on the dynamics of concentrated colloidal hard-sphere dispersions has been reported. There it has been shown that gravity significantly influences aging dynamics if the gravitational length to particle diameter ratio becomes of order 10 or smaller. In the system studied here, the gravitational length to particle diameter ratio is approximately 9, while in Ref. [8] it is roughly 100. The one in the system of swollen microsponges studied in Ref. [7] probably is even larger than that. Yet, we have no reason to believe that gravity is qualitatively important here. Indeed, in Ref. [21] it has been shown that gravity effects become important after much longer waiting times than the ones in this study. Moreover, our results on particle displacements Figs. 2 and 3 clearly indicate that gravity does not qualitatively influence the devitrification scenario as reported by the light scattering studies. We therefore have no reason to believe that gravity qualitatively influences the coupling to static structure upon devitrification either.

IV. CONCLUSIONS

The sequence of repulsive glass–devitrified state–attractive glass was observed in concentrated suspensions of colloidal spheres as a function of increasing interparticle attraction, in agreement with Refs. [6,7]. We have shown that devitrification in real space is significantly reflected in broadening of the displacement distribution and its moments. Displacement distributions are non-Gaussian. The shapes of the displacement distributions are not significantly different for the two different glass states and the devitrified state. The last observation is reflected in the value of the non-Gaussian parameter α_2. Analysis of structure and local density fluctuations revealed no significant differences between the three situations. Considering our experimental setup, this implies that relative density fluctuations are at most a few percent of the average interparticle distance. Obviously, dynamically, a clear signature of devitrification and revitrification occurs, but we do not find significant differences in local structure and density distributions in real space.

ACKNOWLEDGMENTS

This work was financially supported by NWO-CW, FOM, and SFB-TR6.

[1] C. A. Angell, Science **267**, 1924 (1995).
[2] P. N. Pusey and W. van Megen, Nature (London) **320**, 340 (1986).
[3] W. Götze, in *Liquids, Freezing, and the Glass transition*, edited by J. P. Hansen, D. Levesque, and J. Zinn-Justin (North-Holland, Amsterdam, 1991).
[4] J. Bergenholtz, W. C. K. Poon, and M. Fuchs, Langmuir **19**, 4493 (2003).
[5] K. Dawson, G. Foffi, M. Fuchs, W. Gotze, F. Sciortino, M. Sperl, P. Tartaglia, T. Voigtmann, and E. Zaccarelli, Phys. Rev. E **63**, 011401 (2000).
[6] K. N. Pham, A. M. Puertas, J. Bergenholtz, S. U. Egelhaaf, A. Moussad, P. N. Pusay, A. B. Schofield, M. E. Cates, M. Fuchs, and W. C.K. PoonScience **296**, 104 (2002).
[7] T. Eckert and E. Bartsch, Phys. Rev. Lett. **89**, 125701 (2002).
[8] K. N. Pham, S. U. Egelhaaf, P. N. Pusey, and W. C. K. Poon, Phys. Rev. E **69**, 011503 (2004).
[9] A. M. Puertas, M. Fuchs, and M. E. Cates, Phys. Rev. Lett. **88**, 098301 (2002).
[10] S. Asakura and F. Oosawa, J. Chem. Phys. **22**, 1255 (1954).
[11] A. Vrij, Pure Appl. Chem. **48**, 471 (1976).
[12] R. P. A. Dullens, E. M. Claesson, D. Derks, A. van Blaaderen, and W. K. Kegel, Langmuir **19**, 5963 (2003).
[13] R. P. A. Dullens, E. M. Claesson, and W. K. Kegel, Langmuir **20**, 658 (2004).
[14] W. K. Kegel and A. van Blaaderen, Science **287**, 290 (2000).
[15] E. H. A. de Hoog, W. K. Kegel, A. van Blaaderen, and H. N. W. Lekkerkerker, Phys. Rev. E **64**, 021407 (2001).
[16] J. C. Crocker and D. G. Grier, J. Colloid Interface Sci. **179**, 298 (1996).
[17] B. R. A. Nijboer and A. Rahman, Physica (Amsterdam) **32**, 415 (1966).
[18] E. R. Weeks, J. C. Crocker, A. C. Levitt, A. Schofield, and D. A. Weitz, Science **287**, 672 (2000).
[19] J. P. Hansen and I. R. McDonald, *Theory of Simple Liquids*, 2nd ed. (Academic Press, London, 1986).
[20] H. N. W. Lekkerkerker, W. C. K. Poon., P. N. Pusey, A. Stroobants, and P. B. Warren, Europhys. Lett. **20**, 559 (1992).
[21] N. B. Simeonova and W. K. Kegel, Phys. Rev. Lett. **93**, 035701 (2004).